Meenakshi Bansal[1], Pardeep Kaur[2], Harmanpreet Kaur[3], Asha Bhatt[4]*

[1]School of Engineering and Technology (SET), CGC University, Mohali , Punjab, India, [2]Department of Physics, Sri Guru Granth Sahib World University, Fatehgarh Sahib , Punjab, India, [3]Department of Physics, University Institute of Sciences, Chandigarh University, Mohali, Punjab, India, [4]Department of Applied Sciences, Indo Global College, Abhipur, Pb, India

Scientific paper
ISSN 0351-9465, E-ISSN 2466-2585
https://doi.org/10.62638/ZasMat1712



Zastita Materijala 67 ()
(2026)

Evaluation of radiation shielding parameters in Eu^{3+}-doped bismuth phosphate glass system

ABSTRACT

This study investigates the gamma-ray shielding and sensing capabilities of Eu^{3+}-doped bismuth phosphate glasses synthesized via the melt-quench method. Physical properties, including density and molar volume, were analyzed experimentally, showing a slight increase in density with Eu^{3+} ion doping. Gamma-ray attenuation properties were examined in a wide energy range (1 keV to 100 GeV) using WinXCom software, evaluating key parameters such as mass attenuation coefficient (μ_m), effective atomic number (Z_{eff}), and mean free path (mfp). The results indicate that Eu^{3+} doping improves radiation shielding efficiency by reducing thickness normalization parameters such as the half value layer (HVL) and the tenth value layer (TVL). Furthermore, exposure build-up factor (EBF) and energy absorption build-up factor (EABF) show variations with increasing Eu^{3+} concentration, suggesting improved sensing capabilities. A comparative analysis between experimental and theoretical values confirms the suitability of Eu^{3+}-doped glasses as effective shielding and sensing materials for gamma radiation applications.

Keywords: *Phosphate glasses, heavy metal oxides, radiation shielding, radiation sensing*

1. INTRODUCTION

The demand for effective radiation shielding materials has significantly increased due to their critical role in protecting humans, animals, and the environment from harmful exposure to ionizing radiation. Gamma rays, widely utilized in radiotherapy, nuclear power plants, and industrial applications, require shielding materials with optimized atomic structure and high durability to attenuate the radiation efficiently [1-3].

Traditionally, concrete has been the primary material for radiation shielding due to its affordability and ease of availability [4]. However, despite its widespread use, concrete exhibits notable drawbacks, including cracking after prolonged exposure, mechanical degradation due to water retention, and opacity, which limits its potential applications in radiation sensing [5-6]. While lead-based shielding materials provide excellent attenuation, their toxicity and weight constraints necessitate alternative solutions, particularly for applications requiring lightweight, transparent, and tuneable shielding materials.

Glass-based shielding materials have emerged as promising candidate due to their ability to incorporate rare-earth ions, which enhance gamma-ray attenuation while maintaining optical transparency. Heavy metal oxide (*HMO*)-based glasses, which contain more than 50 mol% heavy metal cations, fulfill key shielding criteria. Common *HMO* glass compositions such as TeO_2, Sb_2O_3, Bi_2O_3, Ga_2O_3, and PbO [7] exhibit exceptional mechanical, thermal, and chemical stability, alongside a high refractive index and dielectric constant, making them suitable for fiber optics, sensors, lasers, optical windows, prisms, and nonlinear optical applications [8-15]. From a shielding perspective, Shamshad*et al.* established that oxide glasses outperform oxyfluoride compositions due to their higher attenuation coefficients and lower HVL values [16]. It is further noted that the inclusion of heavy metals in oxyfluoride glasses resulted in increased refractive index and broad optical transparency. P. Kaur*et al.*

*Corresponding author: Pardeep Kaur
Email: p.kaur94653@gmail.com
Paper received: 25. 05 2026.
Pape corrected: 11. 06. 2026.
Pape accepted: 20. 06. 2026.

validated the superior gamma-ray shielding potential of heavy-metal oxide glasses, reinforcing their applicability in high-radiation environments [17].

In addition to *HMOs*, lanthanides enhance the physical, chemical, and thermal characteristics of glass networks, particularly improving chemical durability. Their higher field strength compared to conventional modifiers contributes to structural stability and resistance to environmental degradation [18]. Europium (Eu^{3+})-doped phosphate glasses are particularly promising due to their ability to simultaneously improve radiation shielding and exhibit luminescence properties relevant for radiation sensing applications [19-23]. Previous investigations on rare-earth-doped glasses have highlighted significant advancements in shielding and sensing capabilities. J.M. Park *et al.* found that Bismuth borate glasses doped with Dy_2O_3, Nd_2O_3, and Sm_2O_3 exhibited noticeable luminescence, while M.M. Smedskjaer*et al*. demonstrated that photoluminescence efficiency could be tuned via heat treatment conditions [24-25]. R.S. Gedam*et al.* reported that La_2O_3 and Nd_2O_3 doping in lithium borate glasses enhanced density and refractive index while decreasing optical band gap and radiation length. Further studies have investigated the structural and spectroscopic behavior of rare-earth-doped borate glasses. Rajesh and colleagues analyzed strontium lithium bismuth borate glasses doped with Pr^{3+}, Nd^{3+}, Dy^{3+}, Sm^{3+}, and Er^{3+}, reporting a reduction in Dy^{3+} emission intensity due to energy transfer mechanisms at concentrations beyond 0.5 mol% [26-29].

Despite these advancements,recent work has looked at many new glass systems for radiation shielding. For example, adding HfO_2 to boro-tellurite glasses improved both gamma and neutron shielding [30]. In bio-glasses, B_2O_3 increased molar volume but lowered shielding efficiency because of its lower atomic number [31]. Studies on bismuth boro-tellurite glasses doped with Tm_2O_3 showed better attenuation and neutron dose absorption [32]. The use of WO_3 in borate-tellurite glasses also improved hardness and shielding ability [33]. Other work has reported effective photon attenuation in Cr_2O_3-doped borosilicate glasses [34]. Beyond glasses, researchers have also explored steels [35] and thin films [36] for radiation protection. Together, these studies show how changing the composition of materials can strongly influence their shielding performance.

Using a combination of experimental measurements and theoretical modeling via WinXCom software, this study examines mass attenuation coefficient, effective atomic number, mean free path, and thickness normalization factors across a broad energy range (1 keV–100 GeV). By establishing the influence of Eu^{3+} concentration on shielding efficiency, this research provides insights into potential applications in radiation protection technologies, including medical imaging, nuclear reactor shielding, and aerospace radiation mitigation systems.

2. EXPERIMENTAL/ MATERIALS AND METHODS

The Eu^{3+}-doped bismuth phosphate glasses were synthesized via the conventional melt-quench method, as described in our earlier work [37]. High-purity oxides and phosphates were weighed according to the nominal composition formula:

$$x\,Eu_2O_3–20\,BaO–20\,Bi_2O_3–1.5\,Al_2O_3–(58.5−x)\,P_2O_5, x = 0,0.5,1.0,1.5\,mol\%$$

The batch mixtures were melted in alumina crucibles at 1100 °C for 1 h, followed by quenching on a preheated steel plate and annealing at 350 °C to remove internal stresses.

For convenience, the samples are denoted by shorthand labels such as 0.0-EuBiPBa, 0.5-EuBiPBa, etc. The prefix indicates the molar fraction of Eu_2O_3 incorporated into the base composition. To ensure clarity and transparency, the complete nominal compositions are summarized in Table 1. Although these values were reported previously [37], they are reproduced here to make the present manuscript self-contained.

Table 1. Nominal compositions of Eu^{3+}- doped bismuth phosphate glasses (Compositions reproduced for clarity)

Sample Label	Eu_2O_3 (mol%)	BaO (mol%)	Bi_2O_3 (mol%)	Al_2O_3 (mol%)	P_2O_5 (mol%)
0.0-EuBiPBa	0	20	20	1.5	58.5
0.5-EuBiPBa	0.5	20	20	1.5	58
1.0-EuBiPBa	1	20	20	1.5	57.5
1.5-EuBiPBa	1.5	20	20	1.5	57

3. GEOMETRY SETUP AND INTENSITY DETERMINATION

To accurately assess the gamma-ray shielding properties of Eu^{3+}-doped bismuth phosphate glasses, experimental measurements were conducted using a narrow beam geometry setup. This configuration minimizes the effects of scattered radiation, ensuring precise intensity measurements. Two radiation sources Cs-137 (662 keV) and Co-60 (1172 keV, 1332 keV) were employed, with spectral data recorded using a DP5GAmptek detector system [38-39].

To optimize beam collimation and avoid unwanted scattering, Midgley conditions were implemented, ensuring a controlled divergence angle (ranging from 0.89º to 1.04º) and a narrow scattering angle (1.70º–1.85º). Lead shielding blocks were strategically positioned around the setup to further eliminate secondary radiation interference [40]. The acquired intensity spectra for varying Eu^{3+} concentrations were then analyzed to determine key attenuation parameters, including μ_m, Z_{eff}, *mfp*. These measurements provide critical insights into the material's shielding efficiency and sensing capability.

Radiation shielding properties have been measured with the use of narrow beam geometry for two different sources, namely Cs^{137} and Co^{60} [41,42]. The geometry setup has been shown in Fig.1 consisting of lead blocks, detector, source, sample and laptop which usesDP5GAmptek software in order to record the spectrum. Midgley conditions have been employed to achieve required narrowness in the geometry setup. Based on thickness range the divergence angle (θ_{out}) ranges from 0.89º to 1.04ºsuch that the scattering angle (θ_{sc}) satisfies the Midgley [43] condition i.e.,θ_{sc} = 1.70º -1.85º. To prevent the beam from scattering the setup has also been sheltered with the use of lead blocks. The experimental results for the Eu^{3+} doped bismuth phosphate glasses are shown through Fig. 2.



Figure 1. Midgley's geometry setup

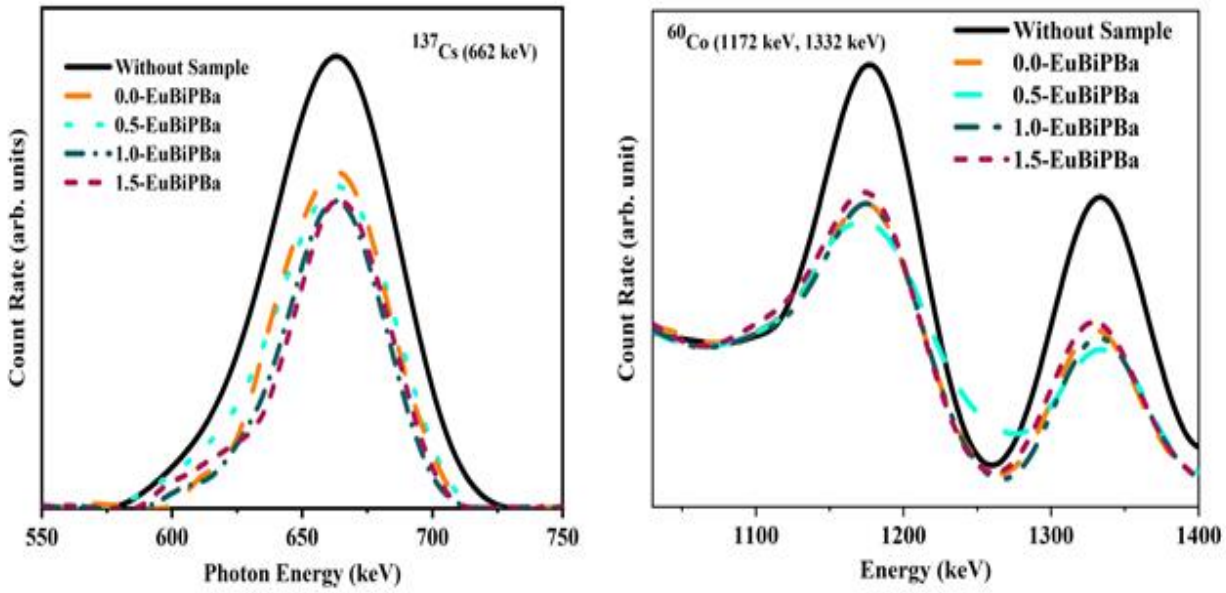

Figute 2. Experimental gamma ray photon intensities with increasing Eu^{3+} concentration

4. REESULTS AND DISCUSSION

4.1. Optimum thickness

Table 2 (given below) presents the optimum thickness values ranging from 1.21 cm to 2.97 cm, demonstrating an increase with photon energy.

Table 2. Optimum thickness range for different samples at different radiation sources

SampleLabel	Optimum Thickness range		Cs^{137}, (662 keV)	Co^{60}, (1172 keV)	Co^{60}, (1332 keV)
0.0-EuBiPBa	X_{min}	$\frac{0.5}{\mu}$	1.27	1.96	2.12
	X_{max}	$\frac{0.7}{\mu}$	1.78	2.74	2.97
	X_{exp}		1.33	2.51	2.51
0.5-EuBiPBa	X_{min}	$\frac{0.5}{\mu}$	1.21	1.87	2.02
	X_{max}	$\frac{0.7}{\mu}$	1.70	2.62	2.83
	X_{exp}		1.29	2.31	2.31
1.0-EuBiPBa	X_{min}	$\frac{0.5}{\mu}$	1.21	1.87	2.02
	X_{max}	$\frac{0.7}{\mu}$	1.70	2.62	2.83
	X_{exp}		1.25	2.22	2.22
1.5-EuBiPBa	X_{min}	$\frac{0.5}{\mu}$	1.21	1.87	2.02
	X_{max}	$\frac{0.7}{\mu}$	1.70	2.62	2.83
	X_{exp}		1.25	2.22	2.22

The highest thickness is observed in the undoped glass sample, while the introduction of rare-earth (RE) ions leads to a noticeable reduction. However, beyond a certain concentration, the decrease stabilizes, likely due to minimal variation in Eu^{3+} incorporation affecting density.

4.2. Physical Parameters

The density of the investigated samples was determined in accordance with Archimedes' principle. The measured density values ranged from 4.31 to 4.61 g/cm³, while the corresponding molar volume varied between 48.32 and 45.81 cm³/mol. These results are consistent with those reported in a previous study [37].

4.3. Mass attenuation coefficient (μ_m)

Figure 3 illustrates the energy-dependent variation of μ_m, categorizing it into three distinct interaction regions.

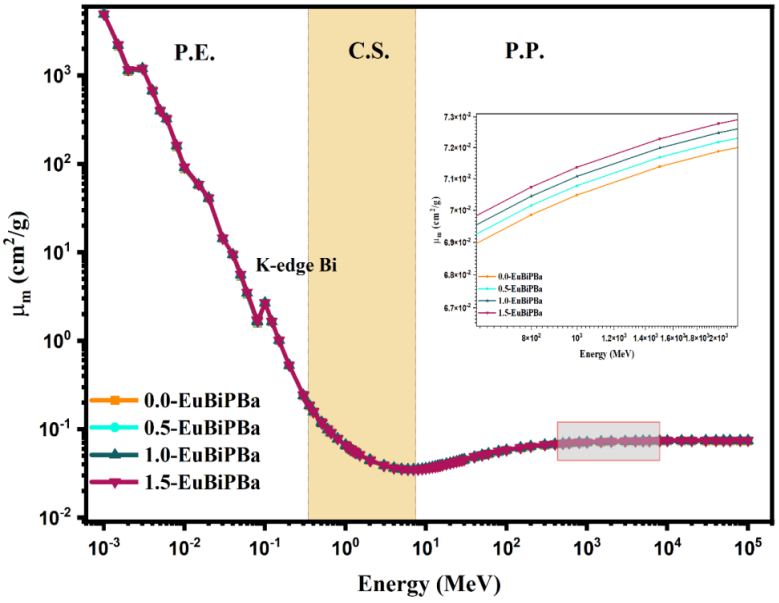

Figure 3. Theoretical values of μ_m for different samples at different radiation energies

The *Eu^{3+}*-doped and undoped glasses exhibit similar trends across all energies, with a notable improvement in attenuation properties due to doping. The μ_m values show an exponential decrease up to 0.35 MeV, followed by minor reductions in the Compton scattering (*CS*) region, where cross-section and energy share an inverse relationship.

In the pair production (*PP*) region, a slight increase occurs due to its Log E dependency. The K absorption edge, closely aligning with Bismuth's edge at 0.093 MeV, further supports the theoretical predictions obtained via WinXCom [44].

Figure 4 comparative analysis of experimental and theoretical values of μ_m for different photon energies such as Cs^{137}- 662 keV and Co^{60}-(1173 keV, 1332 keV). The theoretical and experiments results are in good agreement with values lying close to each other.

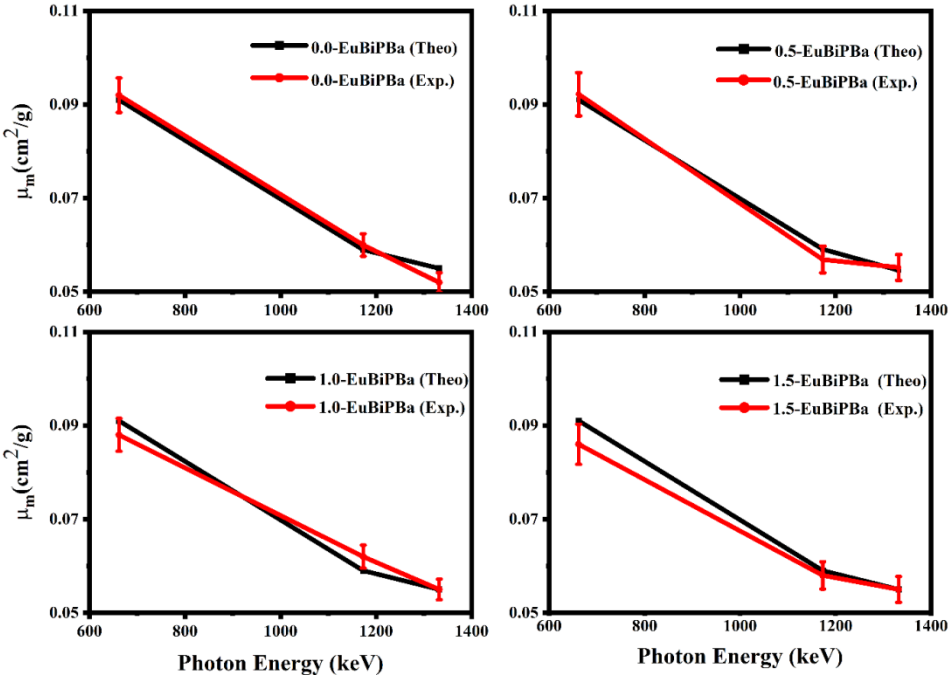

Figure 4. Comparison of experimental and theoretical values of μ_m for different samples at different radiation energies

The $\mu_m$values are displayed in Table 3 which doesn't vary much with the doping concentration as they are density dependent. The density of prepared glasses remains nearly constant as the doping concentration in very less with Europium possessing similar atomic number. Down the column, μ_m values follow decreasing trend with increase in energy values.

Table 3. Theoretical and experimental values of μ_m for different samples at different radiation sources

Energy (keV)	Mass attenuation coefficient (μ_m)	0.0-EuBiPBa	0.5-EuBiPBa	1.0-EuBiPBa	1.5-EuBiPBa
Cs^{137} (662 keV)	$(\mu_m)_{theo.}$	0.0911	0.0910	0.0911	0.0911
	$(\mu_m)_{exp.}$	0.0924	0.0922	0.0880	0.0859
	S.D.	±0.0188	±0.0049	±0.0014	±0.0200
	Percentage Deviation	-2.22	-1.32	3.35	4.81
Co^{60} (1173 keV)	$(\mu_m)_{theo.}$	0.0592	0.0591	0.0591	0.0591
	$(\mu_m)_{exp.}$	0.0596	0.0569	0.0620	0.0579
	S.D.	±0.0106	±0.0052	±0.0095	±0.0074
	Percentage Deviation	-1.29	3.57	-5.33	1.82
Co^{60} (1332 keV)	$(\mu_m)_{theo.}$	0.0547	0.0546	0.0547	0.0546
	$(\mu_m)_{exp.}$	0.0522	0.0552	0.0554	0.0555
	S.D.	±0.0032	±0.0038	±0.0048	±0.0049
	Percentage Deviation	4.58	-1.13	-1.41	-1.63

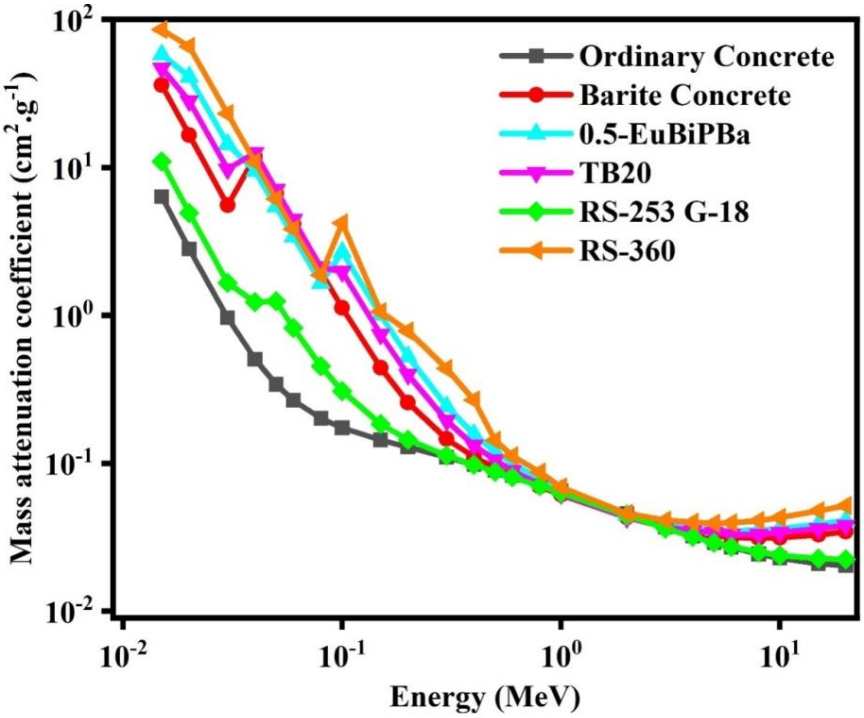

Figure 5. Variation of mass attenuation coefficient (μ/ρ) with photon energy for 0.5-EuBiPBa compared with ordinary concrete, barite concrete, TB20, RS-253 G-18, and commercial RS-360 glass.

In this study, a comparative analysis was carried out between the prepared Eu^{3+}-doped bismuth phosphate glass (0.5-EuBiPBa) and other shielding materials, including ordinary concrete, barite concrete, RS-253 G-18, TB20, and RS-360. The comparison, based on mass attenuation coefficient values, is shown in Fig. 5. The results reveal that the EuBiPBa glass exhibits the highest μ/ρ values across the studied energy range. In descending order, the performance of the other materials was TB20, barite concrete, RS-253 G-18, RS-360, and ordinary concrete. The superior attenuation of the EuBiPBa glass highlights its effectiveness as a radiation shielding material and demonstrates its potential as a lead-free alternative to conventional concretes and commercial glasses.

4.4. Effective atomic number (Z_{eff})

The term Z_{eff} is used to specify the atomic number of composite materials like glasses through a single value and helps in determining their radiation protection ability [45]. **Fig. 6** illustrates the behavior of Z_{eff} curves with the variation of photon energy from 1keV to 100GeV. Most significant Z_{eff} values have been observed for the sample with the maximum doping concentration of Eu^{3+} ions.

Similar to μ_m values the interaction mechanisms effect the Z_{eff} values such that these values have maxima in the P.E. region ($\sigma_{PE} \propto Z^{4-5}$) and minima in the *CS* region. In the P.P. region, Z_{eff} values were found to increase again as the cross-section varied by the factor Z^2. Table 4 presents a comparative analysis of theoretical and experimental Z_{eff} values for different energy sources. The values of Z_{eff} are found to be increasing with an increase in the Eu^{3+} ion concentration. The error, expressed as percentage deviation, was determined to be under 5%, indicating that the measured values are in close agreement with the expected results and validating the reliability of the experimental procedure.

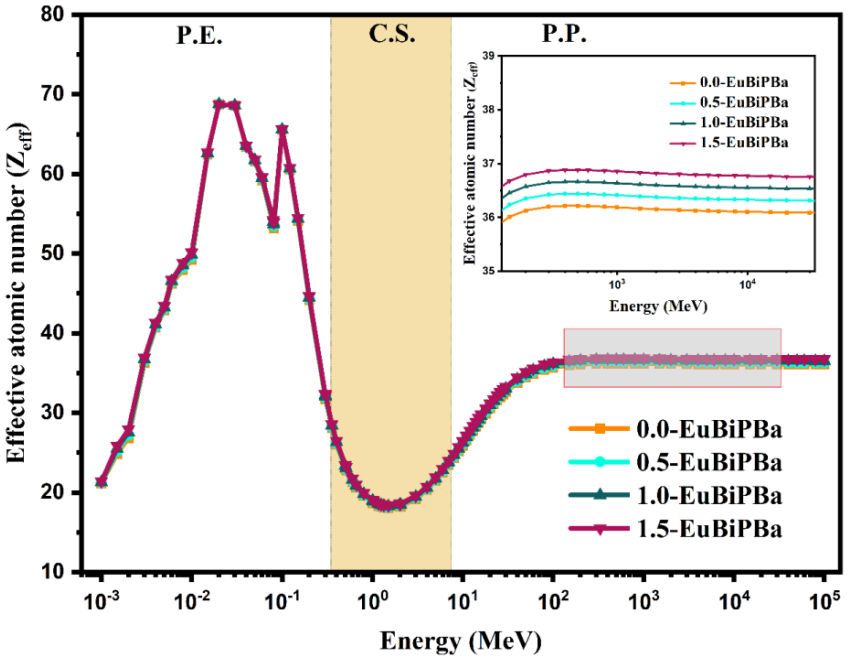

Figure 6. Theoretical values of Z_{eff} for different samples at different radiation energies

Table 4. Theoretical and experimental values of Z_{eff} for different samples at different radiation sources

Energy (keV)	Effective atomic number (Z_{eff})	0.0-EuBiPBa	0.5-EuBiPBa	1.0-EuBiPBa	1.5-EuBiPBa
Cs^{137} (662 keV)	$(Z_{eff})_{theo}$	20.63	20.76	20.88	21.00
	$(Z_{eff})_{exp}$	20.93	21.01	20.18	19.81
Co^{60} (1172 keV)	$(Z_{eff})_{theo}$	18.31	18.42	18.53	18.64
	$(Z_{eff})_{exp}$	18.43	17.71	19.43	18.26
Co^{60} (1332 keV)	$(Z_{eff})_{theo}$	18.11	18.22	18.34	18.44
	$(Z_{eff})_{exp}$	17.28	18.39	18.58	18.73

4.5. Electron density (N_e)

Table 5 compares theoretical and experimental N_e values, revealing close alignment. These values are found to be decreasing with an increase in Eu^{3+} ion concentration.

Table 5. Theoretical and experimental values of Ne for different samples at different radiation

Energy (keV)	Electron Density (N_e), × 10^{23} e/g	0.0-EuBiPBa	0.5-EuBiPBa	1.0-EuBiPBa	1.5-EuBiPBa
Cs^{137} (662 keV)	$(N_e)_{theo.}$	3.32	3.32	3.31	3.31
	$(N_e)_{exp.}$	3.37	3.36	3.20	3.13
Co^{60} (1172 keV)	$(N_e)_{theo.}$	2.95	2.94	2.94	2.94
	$(N_e)_{exp.}$	2.97	2.83	3.08	2.88
Co^{60} (1332 keV)	$(N_e)_{theo.}$	2.92	2.91	2.91	2.92
	$(N_e)_{exp.}$	2.78	2.94	2.95	2.95

Figure 7 illustrates the variation of N_e across the energy range of 1 keV–100 GeV, following a similar trend to Z_{eff}.Although a slight decrease in N_e is observed at higher photon energies, its dependency on μ_m is minimal, likely due to the consistent density of prepared glass samples and the negligible variation in electronic concentration (σ_e) upon Eu^{3+} incorporation. The comparative analysis in Fig. 8 further supports this observation.

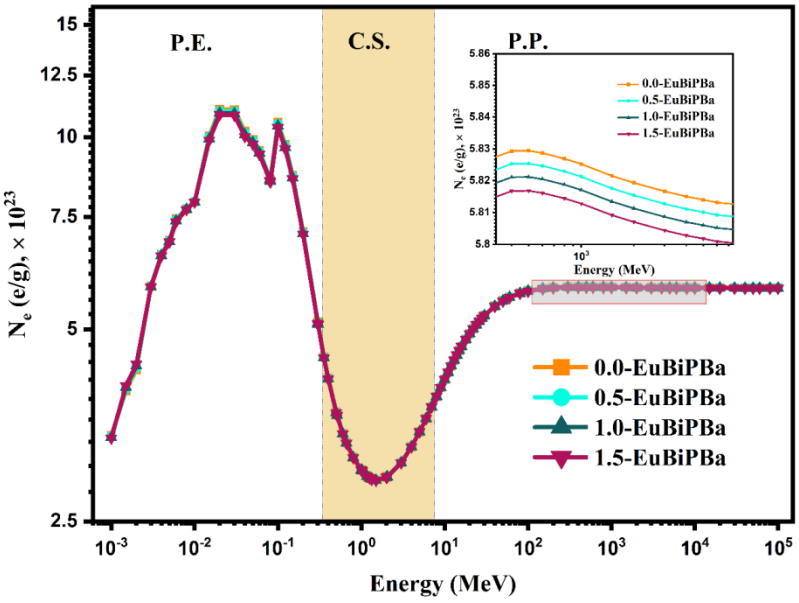

Figure 7. Theoretical values of N_e for different samples at different radiation energies

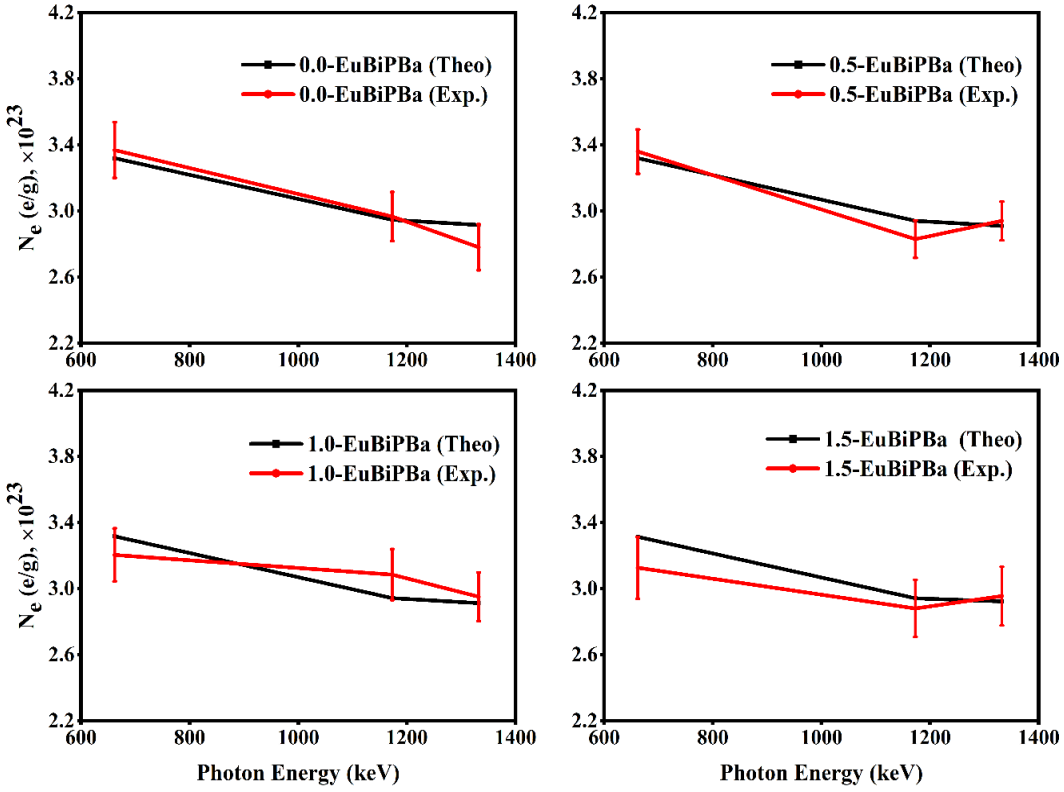

Figure 8. Comparison of experimental and theoretical values of N_e for different samples at different radiation energies

4.6. Thickness normalizing parameters (mfp, HVL and TVL)

In order to access the radiation shielding ability of material, thickness plays an important role. The thickness normalizing parameters for the prepared glass samples were computed and demonstrated using Figure 9. The *mfp, HVL* and *TVL* values keeps on increasing in the photoelectric effect (*PE)* region starting from 1keV and becomes maximum in the *CS* region.

In the P.P. region there is slight decrease in the values. As seen from Table 6, glasses of larger

width were required for the attenuation of high energy gamma radiations.Across the Table 6, it is clear that glasses with lower mfp, HVL and TVL are more effective in stopping the gamma radiation as compared to the higher ones. Among the prepared glass samples, the 1.5–EuBiPBa sample possesses the lowest thickness values.

Table 6. Theoretical and experimental values of mfp, HVL and TVL for different samples at different radiation sources

Energy (keV)	Thickness normalizing parameters (cm)	0.0-EuBiPBa	0.5-EuBiPBa	1.0-EuBiPBa	1.5-EuBiPBa
Cs^{137} (662 keV)	$mfp_{theo.}$	2.55	2.43	2.41	2.38
	$mfp_{exp.}$	2.51	2.40	2.50	2.52
	$HVL_{theo.}$	1.77	1.68	1.67	1.65
	$HVL_{exp.}$	1.74	1.66	1.73	1.75
	$TVL_{theo.}$	5.86	5.59	5.56	5.49
	$TVL_{exp.}$	5.78	5.52	5.75	5.81
Co^{60} (1173 keV)	$mfp_{theo.}$	3.92	3.74	3.72	3.67
	$mfp_{exp.}$	3.89	3.89	3.54	3.75
	HVL_{theo}	2.72	2.59	2.57	2.54
	$HVL_{exp.}$	2.70	2.69	2.46	2.60
	$TVL_{theo.}$	9.03	8.61	8.56	8.45
	$TVL_{exp.}$	8.96	8.95	8.16	8.63
Co^{60} (1332 keV)	$mfp_{theo.}$	4.24	4.04	4.02	3.97
	$mfp_{exp.}$	4.44	4.01	3.97	3.91
	$HVL_{theo.}$	2.94	2.80	2.79	2.75
	$HVL_{exp.}$	3.08	2.78	2.75	2.70
	$TVL_{theo.}$	9.77	9.31	9.26	9.14
	$TVL_{exp.}$	10.23	9.23	9.14	9.00

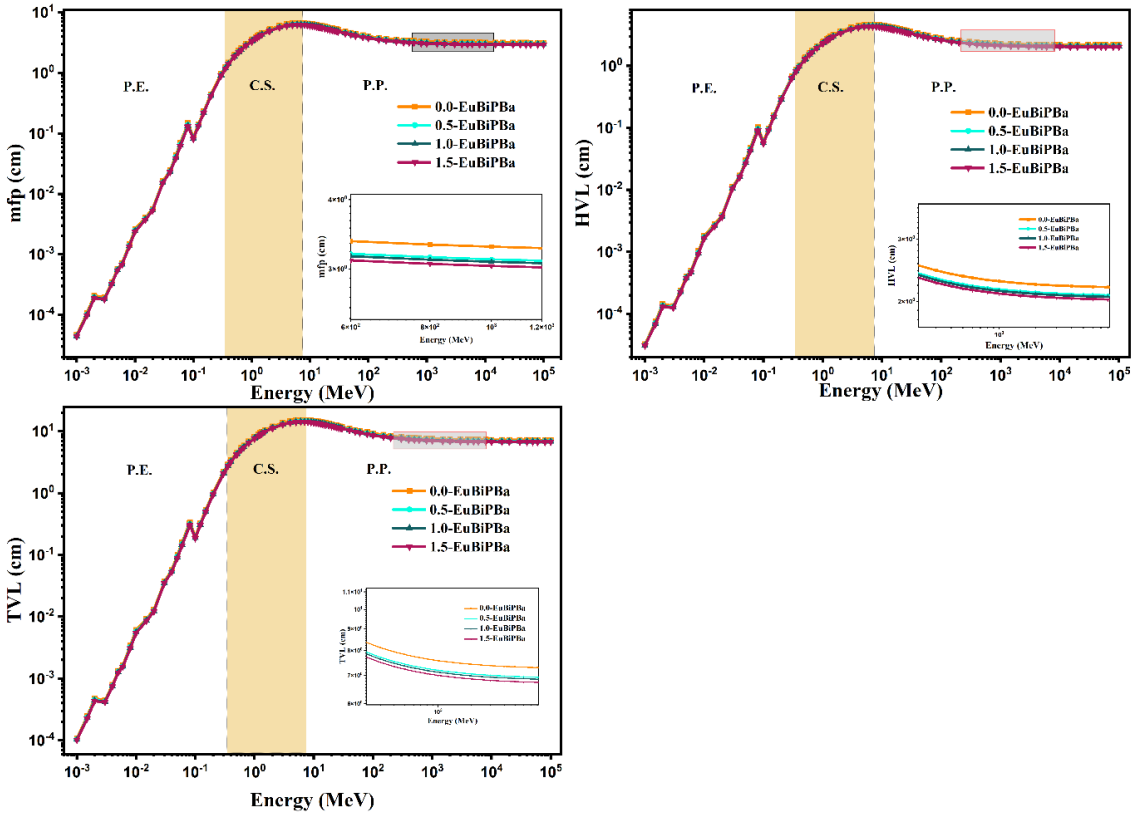

Figure 9. Theoretical values of mfp, HVL and TVL for different samples at different radiation energies

The decrease in thickness normalizing parameters can be ascribed to the large difference in the concentration of Europium and phosphorus, such that it affects the atomic number of the glass. Moreover, decrease in the values of 1.5–EuBiPBa sample with maximum Eu^{3+} ions concentration is due to availability of more particles for photon-particle collisions within the glass structure [46-48]. Fig. 10, Fig. 11 and Fig. 12 describe the comparative investigation of mfp, HVL and TVL respectively.

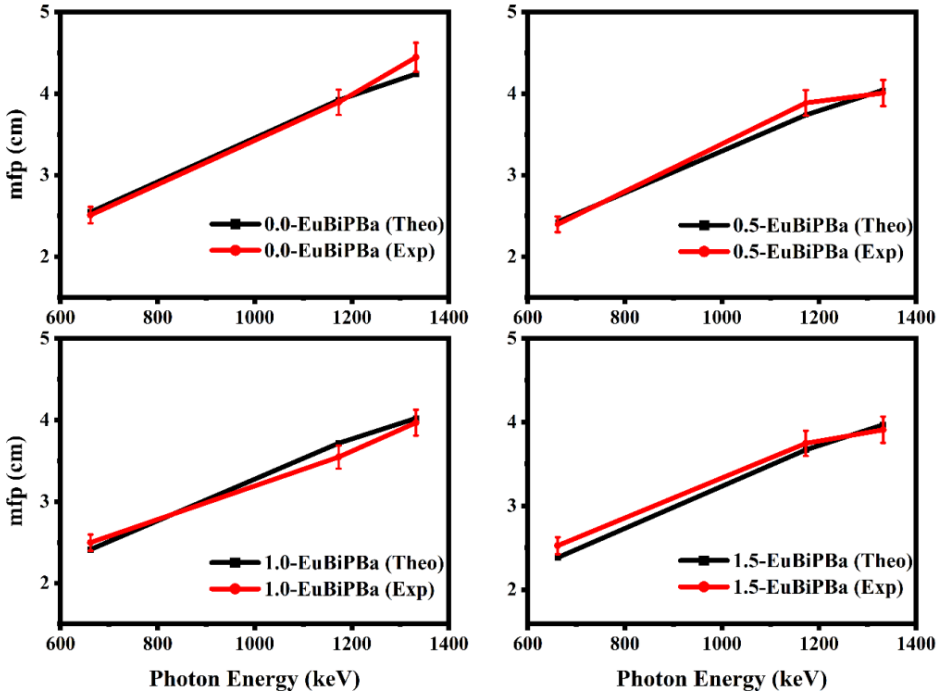

Figure 10. Comparison of experimental and theoretical values of mfp for different samples at different radiation energies

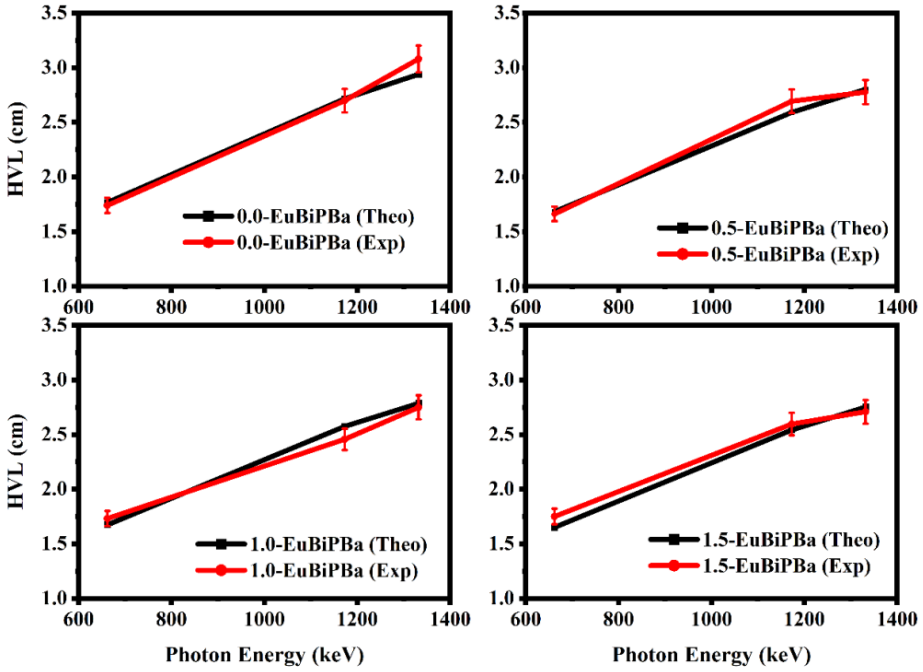

Figure 11. Comparison of experimental and theoretical values of HVL for different samples at different radiation energies

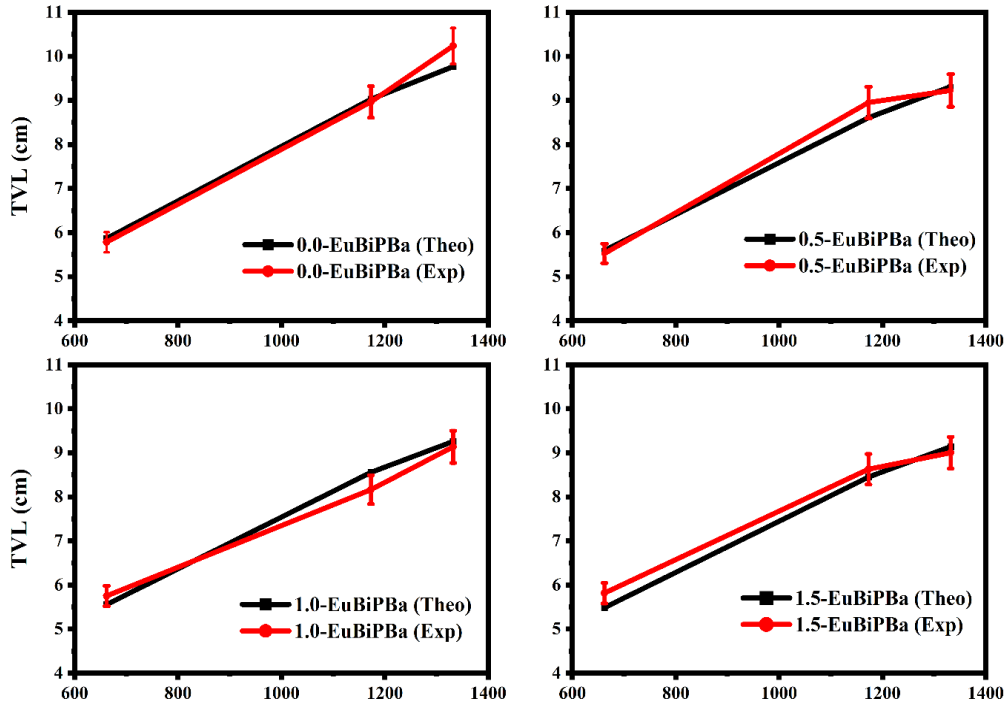

Figure 12. Comparison of experimental and theoretical values of TVL for different samples at different radiation energies

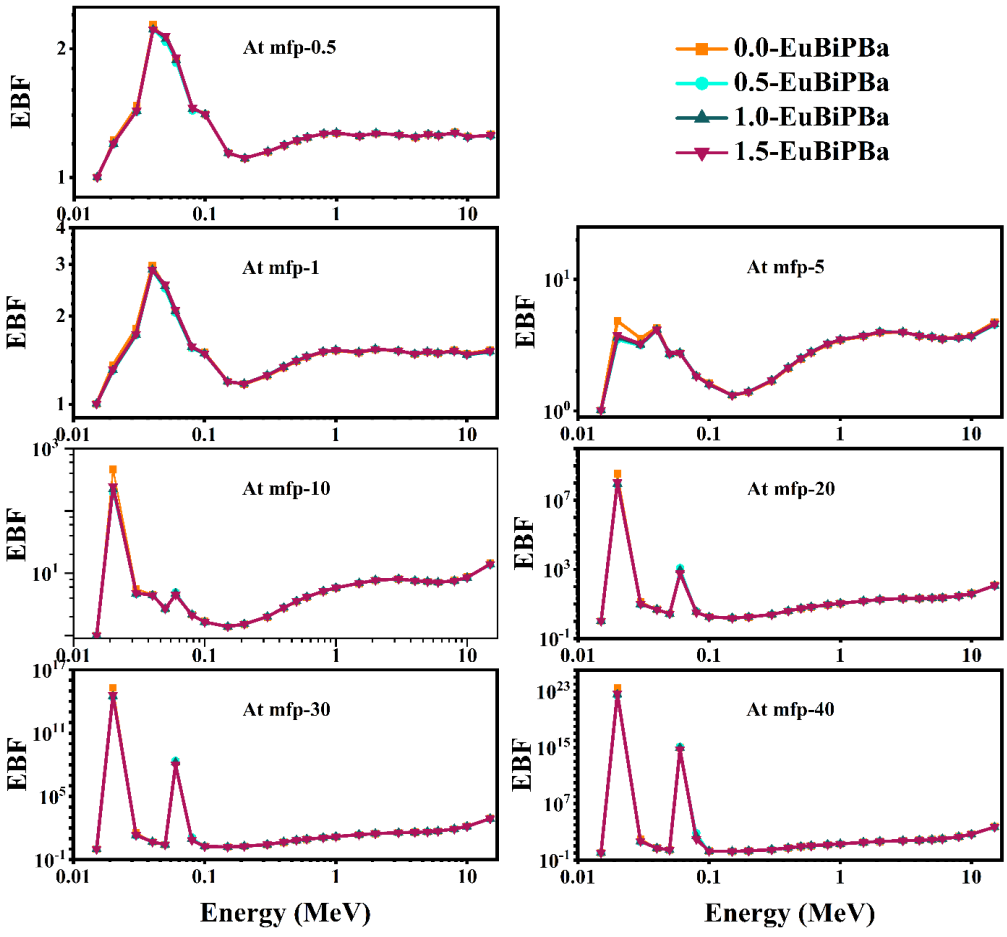

Figure 13. Deviation in the EBF values for increasing thickness

4.7. Build-up factors

4.7.1. EBF analysis

The build-up factor quantifies energy transfer efficiency between gamma photons and shielding materials. **Fig. 13** presents EBF variations with penetration depth, where the lower energy region (~0.037 MeV) exhibits a broad peak, corresponding to the K-edge of Ba. Compositional changes lead to peak splitting, while EBF values systematically rise with increasing *mfp*, signifying enhanced photon interactions.

4.7.2. EABF behavior, highlighting its dependency on multiple Compton collisions

A distinct peak at 0.02 MeV emerges after 5 mfp, corresponding to the K-edge of heavy elements, showing maximum intensity in the undoped sample due to the absence of Eu^{3+} ions. At higher photon energies, *EABF* values further increase due to pair production dominance. The greater atomic number of the present composition contributes to higher photon-atom interactions, resulting in increased *EABF* compared to *EBF*. However, upon Eu^{3+} doping, a noticeable reduction in build-up factors occurs, reinforcing its efficiency as a shielding material.

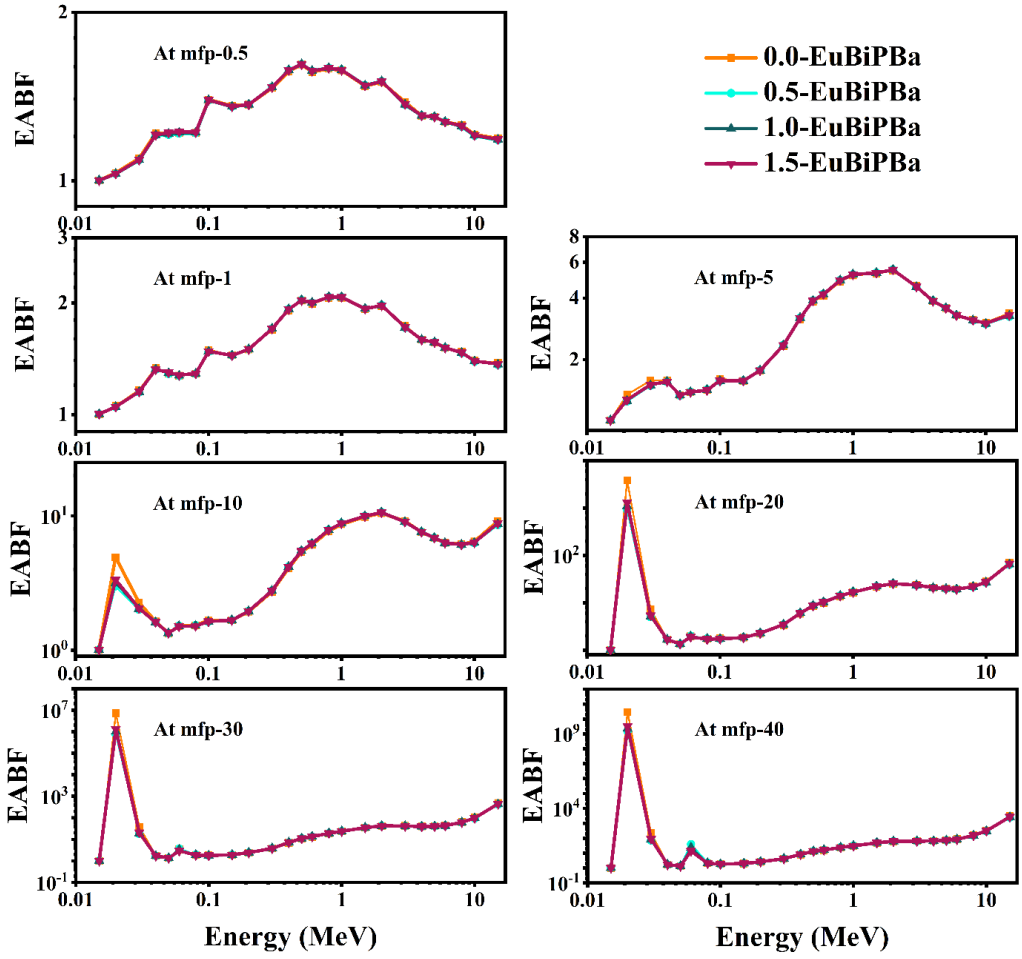

Figure 14. Deviation in the EABF values for increasing thickness

5. CONCLUSION

The study systematically evaluated Eu^{3+}-doped and undoped bismuth phosphate glasses in terms of gamma-ray attenuation properties. The μ_m values exhibit a noticeable improvement in doped samples, with reduced photoelectric absorption edges and enhanced attenuation in higher energy regions. Comparisons between experimental and theoretical values indicate strong alignment, reinforcing the reliability of both methods in assessing shielding performance.

Moreover, the thickness normalizing parameters (*mfp, HVL, TVL*) demonstrate a clear advantage in Eu^{3+}-doped glasses, as lower values

signify improved radiation shielding. The undoped samples require a greater thickness to attenuate gamma radiation, whereas doping reduces the required material thickness due to increased photon interaction probability.

In terms of build-up factors (*EBF and EABF*), doped glasses exhibit lower values, indicating better photon absorption and reduced secondary scattering effects compared to their undoped counterparts. This suggests that Eu^{3+}-doped compositions enhance shielding efficiency by limiting gamma photon transmission beyond the material surface.

Overall, the comparative analysis confirms that Eu^{3+} incorporation significantly improves radiation attenuation, offering a promising alternative to conventional shielding materials. These findings establish the doped glasses as viable candidates for applications in nuclear safety, medical imaging, and advanced radiation detection technologies.

6. REFERENCES

[1] M. I. Sayyed, K. M.Kaky, E.Şakar, U. Akbaba, M. M. Taki, O.& Agar (2019). Gamma radiation shielding investigations for selected germanate glasses. *Journal of Non-Crystalline Solids*, *512*, 33-40.https://doi.org/10.1016/j.jnoncrysol.2019.02.014

[2] V. P. Singh, N. M. Badiger, J.Kaewkhao (2014). Radiation shielding competence of silicate and borate heavy metal oxide glasses: comparative study. *Journal of non-crystalline solids*, *404*, 167-173.https://doi.org/10.1016/j.jnoncrysol.2014.08.003

[3] R. Bagheri, A. K. Moghaddam, S. P. Shirmardi, B. Azadbakht, M. Salehi, (2018). Determination of gamma-ray shielding properties for silicate glasses containing Bi_2O_3, PbO, and BaO. *Journal of Non-Crystalline Solids*, *479*, 62-71.. https://doi.org/10.1016/j.jnoncrysol.2017.10.006

[4] H. O. Tekin, M. I. Sayyed, S. A. Issa(2018). Gamma radiation shielding properties of the hematite-serpentine concrete blended with WO_3 and Bi_2O_3 micro and nano particles using MCNPX code. *Radiation Physics and Chemistry*, *150*, 95-100. https://doi.org/10.1016/j.radphyschem.2018.05.002

[5] C. M. Lee, Y. H. Lee, K. J. Lee(2007). Cracking effect on gamma-ray shielding performance in concrete structure. *Progress in Nuclear Energy*, *49*(4), 303-312. https://doi.org/10.1016/j.pnucene.2007.01.006

[6] J. Wang K. Sun, Y. Hu, Q. Guan, Q. Li (2022). The mechanical properties of concrete in water environment: A review. Frontiers in Materials, 9, 996650.https://doi.org/10.3389/fmats.2022.996650

[7] K. Ouannes, M. T. Soltani, M. Poulain, G. Boulon, G. Alombert-Goget, Y. Guyot, Y. &K. Lebbou (2014). Spectroscopic properties of Er3+-doped antimony oxide glass. *Journal of alloys and compounds*, *603*, 132-135. https://doi.org/10.1016/j.jallcom.2014.02.008

[8] J. Zavadil, Z. G. Ivanova, P. Kostka, M. Hamzaoui, M. T. Soltani (2014). Photoluminescence study of Er-doped zinc–sodium–antimonite glasses. *Journal of alloys and compounds*, *611*, 111-116. https://doi.org/10.1016/j.jallcom.2014.05.102

[9] M. Soltani, M. Hamzaoui, S. Houhou, H. Touiri, L. Bediar, A. Ghemri, P. Petkova (2013). Physical Characterization of Sb_2O_3-M_2O-MoO_3 (M~= Li,~ K) New Glasses. *Acta Physica Polonica A*, *123*(2), 227-229.https://doi.org/10.12693/APhysPolA.123.227

[10] M. Hamzaoui, S. Azri, M. T. Soltani, R. Lebullenger, M. Poulain (2013). Thermal and elastic characterization of Sb_2O_3–Na_2O–ZnO glasses. *Physica Scripta*, *2013*(T157), 014029. https://doi.org/10.1088/0031-8949/2013/T157/014029

[11] Baazouzi M, Soltani MT, Hamzaoui M, Poulain M, Troles J. Optical properties of alkali-antimonite glasses and purified processes for fiber drawing. Opt. Mater. 2013;36(2):500-4. https://doi.org/10.1016/j.optmat.2013.10.017

[12] M. T. Soltani, A. Boutarfaia, R. Makhloufi, M. Poulain (2003). New alkali antimonate glasses. *Journal of Physics and Chemistry of Solids*, *64*(12), 2307-2312 https://doi.org/10.1016/S0022-3697(03)00220-8

[13] P. Kostka, J. Zavadil, J. Pedlikova, M. Poulain (2011). Preparation and optical characterization of $PbCl_2$–Sb_2O_3–TeO_2 glasses doped with rare earth elements. *physica status solidi (a)*, *208*(8), 1821-1826. https://doi.org/10.1002/pssa.201084098

[14] R. A. El-Mallawany (2002). Applications of Tellurite Glasses and Tellurite Glass Ceremics. Tellurite Glasses Handbook. CRC Press;.

[15] F. Goumeidane, M. Legouera, M. Iezid, M. Poulain, V. Nazabal, R. Lebullenger (2011). Synthesis and physical properties of glasses in the Sb_2O_3–$PbCl_2$–MoO_3 system. *Journal of non-crystalline solids*, *357*(21), 3572-3577. https://doi.org/10.1016/j.jnoncrysol.2011.07.012

[16] L. Shamshad, G. Rooh, P. Limkitjaroenporn, N. Srisittipokakun, W. Chaiphaksa, H. J. Kim, J. Kaewkhao (2017). A comparative study of gadolinium based oxide and oxyfluoride glasses as low energy radiation shielding materials. *Progress in Nuclear Energy*, *97*, 53-59. https://doi.org/10.1016/j.pnucene.2016.12.014

[17] P. Kaur, D. Singh, T. Singh (2016). Heavy metal oxide glasses as gamma rays shielding material. *Nuclear Engineering and design*, *307*, 364-376. https://doi.org/10.1016/j.nucengdes.2016.07.029

[18] P. Kaur, D. Singh, T. Singh, P. Kaur (2021, August). Gamma radiation shielding characteristics for some rare earth doped lead borate glasses. In *AIP Conference Proceedings* (Vol. 2352, No. 1, p. 050035). AIP Publishing LLC. https://doi.org/10.1063/5.0053029

[19] P. Kaur, J. Singh, P. Kaur, T. Singh (2023). Radiation shielding and sensing properties for some Eu^{3+} doped bismo-phosphate glasses. *Radiation Physics and Chemistry*, *206*, 110769. https://doi.org/10.1016/j.radphyschem.2023.110769

[20] S. K. Barik, A. Senapati, S. Balakrishnan, K. Ananthasivan (2022). Synthesis and characterization of rare-earth doped aluminium phosphate glasses. *Progress in Nuclear Energy*, *152*, 104372. https://doi.org/10.1016/j.pnucene.2022.104372

[21] T. Yanagida (2016).Ionizing radiation induced emission: scintillation and storage-type luminescence. Journal ofLuminescence. 169,544-548. https://doi.org/10.1016/j.jlumin.2015.01.006

[22] T. Yanagida (2013). Study of rare-earth-doped scintillators. Optical materials. 35(11), 1987-1992. https://doi.org/10.1016/j.optmat.2012.11.002

[23] W. A. Pisarski(2022). Rare earth doped glasses/ceramics: Synthesis, structure, properties and their optical applications. *Materials*, *15*(22), 8099.https://doi.org/10.3390/ma15228099

[24] J. M. Park, H. J. Kim, P. Limsuwan, J. Kaewkhao (2012). Luminescence property of rare-earth-doped bismuth-borate glasses with different concentrations of bismuth and rare-earth material. *Journal of the Korean Physical Society*, *61*(2), 248-253. https://doi.org/10.3938/jkps.61.248

[25] M. M. Smedskjaer, J. Wang, Y. Yue(2011). Tunable photoluminescence induced by thermal reduction in rare earth doped glasses. *Journal of Materials Chemistry*, *21*(18), 6614-6620.https://doi.org/10.1039/c1jm10472a

[26] R. S. Gedam, D. D. Ramteke (2012). Electrical and optical properties of lithium borate glasses doped with Nd_2O_3. *Journal of rare Earths*, *30*(8), 785-789.https://doi.org/10.1016/S1002-0721(12)60130-6

[27] R. S. Gedam, D. D. Ramteke (2013). Electrical, dielectric and optical properties of La_2O_3 doped lithium borate glasses. *Journal of Physics and Chemistry of solids*, *74*(7), 1039-1044. https://doi.org/10.1016/j.jpcs.2013.03.001

[28] K. Brahmachary, D. Rajesh, S. Babu, Y. C. Ratnakaram (2014). Investigations on spectroscopic properties of Pr^{3+} and Nd^{3+} doped zinc-alumino-sodium-phosphate (ZANP) glasses. *Journal of Molecular Structure*, *1064*, 6-14. https://doi.org/10.1016/j.molstruc.2014.01.056

[29] D. Rajesh, Y. C. Ratnakaram, M. Seshadri, A. Balakrishna, T. S. Krishna (2012). Structural and luminescence properties of Dy^{3+} ion in strontium lithium bismuth borate glasses. *Journal of luminescence*, *132*(3), 841-849. https://doi.org/10.1016/j.jlumin.2011.08.050

[30] S. Y. Rasul, B. Aktas, D. Yilmaz, A. F. Pathman, S. Yalcin, A. Acikgoz (2025). Impact of HfO_2 on the structural, thermal, gamma, and neutron shielding properties of boro-tellurite glasses. *Inorganic Chemistry Communications*, 174, 113993. https://doi.org/10.1016/j.inoche.2025.113993

[31] E. O. Ulas, A. Acikgoz, B. Aktas, Y. Kavun (2025), Influence of B_2O_3 incorporation on the structural, mechanical and radiation shielding properties of TeO_2 Based bioglasses. *Applied Radiation and Isotopes*, 221, 111799. 10.1016/j.apradiso. 2025.111799

[32] K. Dogru, B. Aktas, A. Acikgoz, D. Yilmaz, A. F. Pathman, S. Yalcin, G. Demircan (2024),Structural, thermal, and radiation shielding properties of B_2O_3-TeO_2-Bi_2O_3-CdO-Tm_2O_3 glasses: The role of Tm_2O_3. *Ceramics International*, 50(22), 47384-47394.https://doi.org/10.1016/j.ceramint.2024.09.088

[33] B. B. Solak, B. Aktas, D. Yilmaz, S. Kalecik, S. Yalcin, A. Acikgoz, G. Demircan (2024), Exploring the radiation shielding properties of B_2O_3-PbO-TeO_2-CeO_2-WO_3 glasses: A comprehensive study on structural, mechanical, gamma, and neutron attenuation characteristics. *Materials Chemistry and Physics*, 312, 128672. https://doi.org/10.1016/j.matchemphys.2023.128672

[34] B. Aktas, S. Yalcin, K. Dogru, Z. Uzunoglu, D. Yilmaz (2019), Structural and radiation shielding properties of chromium oxide doped borosilicate glass, *Radiation Physics and Chemistry*, 156, 144-149. https://doi.org/10.1016/j.radphyschem.2018.11.012

[35] D. Yılmaz, B. Aktaş, A. Çalık, O.B. Aytar (2019), Boronizing effect on the radiation shielding properties of Hardox 450 and HardoxHiTuf steels. *Radiation Physics and Chemistry*, 161, 55-59. https://doi.org/10.1016/j.radphyschem.2019.04.019

[36] E. B. Buzok, S. Yalcin, G. Demircan, D. Yılmaz, B. Aktas, E. Aytar (2024), The structural, optical, electrical and radiation shielding properties of Co-doped ZnO thin films. *Radiation Physics and Chemistry*, 222, 111840. https://doi.org/10.1016/j.radphyschem.2024.111840

[37] P. Kaur, P. Kaur, T. Singh (2024), Thermal stability and spectroscopic properties of Eu-doped phosphate glasses for lasing applications. *Ceramics International*, 50, 7868–7877. https://doi.org/10.1016/j.ceramint.2023.12.115

[38] Y. C. Ratnakaram, A. Balakrishna, D. Rajesh, M. Seshadri (2012). Influence of modifier oxides on spectroscopic properties of Sm^{3+} doped lithium fluoroborate glass. *Journal of Molecular Structure*, *1028*, 141-147. https://doi.org/10.1016/j.molstruc.2012.05.071

[39] D. Rajesh, Y. C. Ratnakaram, A. Balakrishna (2013). Er^{3+}-doped strontium lithium bismuth borate glasses for broadband 1.5 μm emission–Structural and optical properties. *Journal of alloys and compounds*, *563*, 22-27. https://doi.org/10.1016/j.jallcom.2013.02.055

[40] A. V. Deepa, P. Murugasen, P. Muralimanohar, K. Sathyamoorthy, P. Vinothkumar (2019). A comparison on the structural and optical properties of different rare earth doped phosphate glasses. *Optik*, *181*, 361-367. https://doi.org/10.1016/j.ijleo.2018.12.045

[41] J. Singh, V. Kumar, T. Singh (2020). Synthesis and photon interaction characterizations of some bioactive glasses. *Journal of Non-Crystalline Solids*, *548*, 120328. https://doi.org/10.1016/j.jnoncrysol.2020.120328

[42] P. Kaur, D. Singh, T. Singh (2018). Gamma rays shielding and sensing application of some rare earth

doped lead-alumino-phosphate glasses. *Radiation Physics and Chemistry*, *144*, 336-343. https://doi.org/10.1016/j.radphyschem.2017.09.018

[43] S. Midgley (2006). Angular width of a narrow beam for X-ray linear attenuation coefficient measurements. *Radiation Physics and Chemistry*, *75*(9), 945-953. https://doi.org/10.1016/j.radphyschem.2006.01.008

[44] L. Gerward, N. Guilbert, K. B. Jensen, H. Levring, H. (2001). X-ray absorption in matter. Reengineering XCOM. *Radiation Physics and Chemistry*, *60*(1-2), 23-24. https://doi.org/10.1016/S0969-806X(00)00324-8

[45] E. Kavaz, H. O. Tekin, G. O. K. H. A. N. Kilic, G. Susoy, G. (2020). Newly developed Zinc-Tellurite glass system: an experimental investigation on impact of Ta_2O_5 on nuclear radiation shielding ability.*Journal of Non-Crystalline Solids*, *544*, 120169. https://doi.org/10.1016/j.jnoncrysol.2020.120169

[46] K. S. Shaaban, A. M. Al-Baradi, A. M. Ali(2022). Gamma-ray shielding and mechanical characteristics of iron-doped lead phosphosilicate glasses. *Silicon*, *14*(14), 8971-8979. https://doi.org/10.1007/s12633-022-01702-x

[47] H. Karami, V. Zanganeh, M. Ahmadi (2023). Study nuclear radiation shielding, mechanical and Acoustical properties of TeO_2-Na_2O-BaO-TiO_2 alloyed glasses. *Radiation Physics and Chemistry*, *208*, 110917. https://doi.org/10.1016/j.radphyschem.2023.110917

[48] A. N. D'Souza, M. I. Sayyed, N. Karunakara, H. Al-Ghamdi, A. H. Almuqrin, M. Elsafi, ... S. D. Kamath, (2022). TeO_2–SiO_2–B_2O_3 glasses doped with CeO_2 for gamma radiation shielding and dosimetry application. *Radiation Physics and Chemistry*, *200*, 110233. https://doi.org/10.1016/j.radphyschem.2022.110233

IZVOD

PROCENA PARAMETARA ZAŠTITE OD ZRAČENJA U SISTEMU STAKLA DOPIRANOG BIZMUT FOSFATOM EU^{3+}

Ova studija istražuje mogućnosti zaštite i detekcije gama zraka bizmut fosfatnih stakala dopiranih Eu^{3+} metodom kaljenja rastopom. Fizička svojstva, uključujući gustinu i molarnu zapreminu, analizirana su eksperimentalno, pokazujući blago povećanje gustine uz dopiranje jonima Eu3+. Osobine slabljenja gama zraka ispitane su u širokom energetskom opsegu (od 1 keV do 100 GeV) korišćenjem WinXCom softvera, procenjujući ključne parametre kao što su koeficijent slabljenja mase (m_m), efektivni atomski broj (Zeff) i srednji slobodni put (mfp). Rezultati pokazuju da dopiranje Eu3+ poboljšava efikasnost zaštite od zračenja smanjenjem parametara normalizacije debljine kao što su sloj polovine vrednosti (HVL) i sloj desete vrednosti (TVL). Štaviše, faktor povećanja ekspozicije (EBF) i faktor povećanja apsorpcije energije (EABF) pokazuju varijacije sa povećanjem koncentracije Eu3+, što ukazuje na poboljšane mogućnosti detekcije. Komparativna analiza eksperimentalnih i teorijskih vrednosti potvrđuje pogodnost stakala dopiranih Eu^{3+} kao efikasnih materijala za zaštitu i detekciju gama zračenja.

Ključne reči: *Fosfatna stakla; Oksidi teških metala; Zaštita od zračenja; Detekcija zračenja*

Naučni rad
Rad primljen: 25.05.2026.
Rad korigovan: 11.06.2026.
Rad prihvaćen: 20.06.2026.

© 2026 Authors. Published by Engineering Society for Corrosion. This article is an open access article distributed under the terms and conditions of the Creative Commons Attribution 4.0 International license (https://creativecommons.org/licenses/by/4.0/)